THE ASTROPHYSICAL JOURNAL, 423:L9–L12, 1994 March 1

TOPOLOGICAL ANALYSIS OF *COBE*-DMR COSMIC MICROWAVE BACKGROUND MAPS

SERGIO TORRES[1]
International Center for Relativistic Astrophysics, Università di Roma 1, Piazzale Aldo Moro, 5-00185, Rome, Italy
Received 1993 October 20; accepted 1993 December 16

ABSTRACT

Geometric characteristics of random fields are exploited to test the consistency of density perturbation model spectra with *COBE* data. These CMB maps are analyzed using the number of anisotropy hot spots and their boundary curvature. CMB maps which account for instrumental effects and sky coverage are Monte Carlo generated. These simulations show that a scale-invariant Harrison-Zeldovich primordial Gaussian density fluctuation spectrum is consistent with the data. The CMB fluctuation coherence angle, based on boundary curvature, gives a spectral index $n = 1.2 \pm 0.3$.

Subject heading: cosmic microwave background

1. INTRODUCTION

Gravitational collapse models of structure formation predict that at large angular scales the cosmic microwave background (CMB) will exhibit random fluctuations. The gravitational potential on the surface which last scatter CMB photons (Sachs & Wolfe 1967) is responsible for these fluctuations. Thus, the primordial matter density spectrum determines the amplitudes of these fluctuations which in k-space is $P(k) = |\delta_k|^2$ and can be represented by a power law, $P(k) \propto k^n$, with spectral index n. The inflationary model requires a scale invariant spectrum with $n = 1$ (Harrison 1970; Zeldovich 1972).

$P(k)$ can be inferred from the CMB temperature autocorrelation function (ACF). Alternatively, $P(k)$ models can be tested statistically using the hot spots in CMB maps. The most important advantage of this second approach is that, unlike ACF computations, topological analysis does not assume an ergodic radiation field (Cayón, Martínez-González, & Sanz 1991; Scaramella & Vittorio 1990), and so provides normalization independent power spectrum information. This later analysis can also be used to diagnose nonrandom CMB map components (e.g., foreground signals); as an unbiased coherence angle estimator of an underlying random field (Adler 1981); and to verify the Gaussian nature of primordial fluctuations and thus test structure formation models relying on primordial seeds (e.g. cosmic strings [Bennett, Stebbins, & Bouchet 1992] or texture [Park, Spergel, & Turok 1991]). Also the existence of non-Gaussian sky temperature contributions from nonergodic behavior can be determined using Monte Carlo simulations.

The first year *COBE*-DMR maps (Smoot et al. 1992 and references therein) are topologically analyzed to check their consistency with the Harrison-Zeldovich power spectrum which a preliminary hot spot analysis found to be the case (Gurzadyan & Torres 1993).

2. THE GEOMETRY OF RANDOM FIELDS

The random field excursion set is the domain of all points in which the field takes on values $T \geq T_\nu = \nu\sigma$, where σ and ν are the temperature field standard deviation and threshold, respectively. Topological descriptors which have been used to characterize CMB excursion regions (Sazhin 1985; Vittorio & Juszkiewics 1987; Bond & Efstathiou 1987; Coles & Borrow 1987; Coles 1988a, 1988b; Gott et al. 1990; Martínez-González 1989) are (1) the number of spots with temperature above T_ν, and below $-T_\nu$, N_ν; (2) the mean area of these spots, A_ν; (3) the total spot boundary curvature, or genus G_ν; (4) the contour level lengths, L_ν; (5) the total spot excursion area, a_ν; (6) the number of up crossings (one dimension) and the Euler-Poincaré characteristic (two dimensions; Adler 1981).

Excursion set geometry theory allows some descriptors to be derived analytically. (e.g., For two-dimensional, stationary, isotropic, random, Gaussian fields the geometric properties depend only on the ACF and its second derivative at zero lag.) A more compact representation is the coherence angle, $\theta_c^2 = -C(0)/C''(0)$. The mean number of spots on the 4π surface, the mean genus, and the total excursion set area are

$$\langle N_\nu \rangle = \frac{2}{\pi\theta_c^2} \frac{\exp(-\nu^2)}{\operatorname{erfc}(\nu/\sqrt{2})}; \tag{1}$$

$$\langle G_\nu \rangle = \left(\frac{2}{\pi}\right)^{1/2} \frac{\nu}{\theta_c^2} \exp\left(-\frac{\nu^2}{2}\right); \tag{2}$$

$$\langle a_\nu \rangle = 2\pi \operatorname{erfc}(\nu/\sqrt{2}). \tag{3}$$

The total excursion set area is independent of θ_c and so can be used to identify systematic effects in the data.

3. COMPUTING TOPOLOGICAL DESCRIPTORS

COBE data is apportioned to pixels by projecting the celestial sphere onto a circumscribed sky cube, each cube side being divided into 1024 pixels (Torres et al. 1989). The resulting 6144 pixels, each have $\approx 2\overset{\circ}{.}9 \times 2\overset{\circ}{.}9$ angular dimensions comparable to *COBE*-DMR angular resolution. The pixel face and Cartesian coordinate identifier allow efficient algorithms to be constructed so that the data can be accessed in a form close to that of the original.

Since hot spots are defined in terms of a threshold, ν, a binary map is constructed for each threshold level, a 1 appearing in pixels whose temperature is greater than or equal to T_ν. Hot spots are located on these bit maps by forming tree data structures. When traversing the sky cube the first 1 pixel encountered becomes the root node and all contiguous 1 pixels become nodes of that tree. A tree is completed when all neighboring pixels are 0. The hot spot area is the number of nodes in the tree. The contour level length is found by counting the

[1] On leave from Universidad de los Andes, and Centro Internacional de Física, Bogotá, Colombia.
E-mail: 40174::tores, torres@celest.lbl.gov.

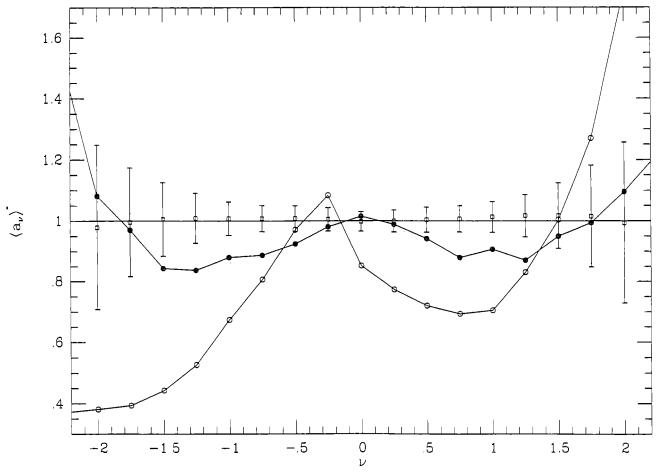

FIG. 1.—Mean value of the total area of excursion divided by $2\pi \operatorname{erfc}(\nu/\sqrt{2})$ at different threshold levels. The horizontal line corresponds to the expected theoretical value for a random field, independent of its coherence angle. Open squares with 1 σ error bars are for Monte Carlo–generated maps. Circles are for the 31(A + B) DMR maps with a 30° (*filled circles*) and a 10° (*open circles*) galactic cut.

neighboring 1 pixels of each node. The total curvature index, or genus, of a bit map is the number of hot spots minus the number of holes (Gott et al. 1992) which are those spots found using the hot spot algorithm recursively on the negative of the bit map minus one.

Simulated Gaussian random field maps are generated and their hot spot number densities and genus, area, and contour lengths evaluated. Figure 1 shows the simulated total area a mean values with theoretical a_ν values, while Figure 2 does the same for genus. The agreement is good.

Excluding the equatorial band to remove contributions from our galaxy introduces a boundary thus enhancing G_ν and N_ν at low thresholds. To account for this artifact all Monte Carlo–generated data sets are treated identically to that of the experimental data.

4. MONTE CARLO SIMULATIONS

A *COBE*-DMR CMB map can be simulated by assigning to each pixel a temperature given by an expansion of real spherical harmonics as defined in Smoot et al. (1991) weighted by the beam filter coefficients W_l. The finite beam width, σ_b, of the instrument enters in W_l as a high-pass filter (Scaramella & Vittorio 1988):

$$W_l = \exp\left[-\tfrac{1}{2}\sigma_b^2 l(l+1)\right] . \quad (4)$$

For random Gaussian fields, the harmonic coefficients of the expansion are random variables with zero mean, are Gaussian distributed, and have variance determined by the primordial matter density perturbation spectrum.

On the scale of the DMR beam ($>2°$) only fluctuations of the gravitational potential on the surface of last scattering affect the CMB isotropy and so the Sachs-Wolfe effect alone suffices to determine the variances. For power-law spectra, $P(k) \propto k^n$, the Bond-Efstathiou formula (1987) for the variances is adequate since only contributions for l up to ~ 30 are important after beam-width filtering and further Gaussian smoothing. Instrumental noise and sky coverage are accounted for by adding to each pixel noise equal to a Gaussian random number with dispersion equal to the noise level per measurement divided by $(N_{\rm obs})^{1/2}$, where the number of observations is included in the original sky maps. To estimate noise for a single measurement the observed temperature squared is apportioned among bins of equal width in $1/N_{\rm obs}$, and the average in each bin is used. The slope of the $\langle T_0^2 \rangle$ versus $1/N$ plot gives the noise level squared. The levels for each channel at each of the three DMR frequencies were within 7% of nominal values.

Two maps are Monte Carlo generated, each with its corresponding noise level, from which sum and difference maps are constructed and 2°.9 Gaussian smoothed. Each sky map produced is one realization of the ensemble from which G_ν, N_ν, A_ν, and L_ν are extracted. After 400 realizations the respective means and dispersions are computed.

Figure 3 shows the means and their 1 σ error bars for the number of hot spots as seen by the 53 GHz DMR radiometer observing a universe with primordial Harrison-Zeldovich fluctuations. Also shown are the spot numbers obtained from maps made with pure instrumental noise. The separation between these two curves indicates both the power of a sta-

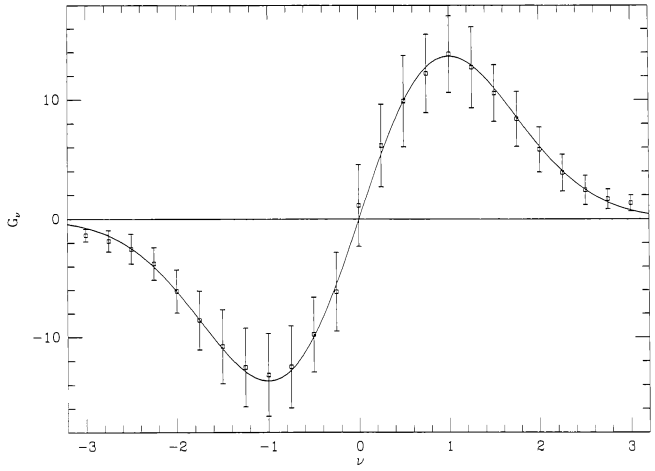

FIG. 2.—Mean values of the genus as a function of threshold for Monte Carlo simulations Gaussian maps. The solid curve is the analytical function.

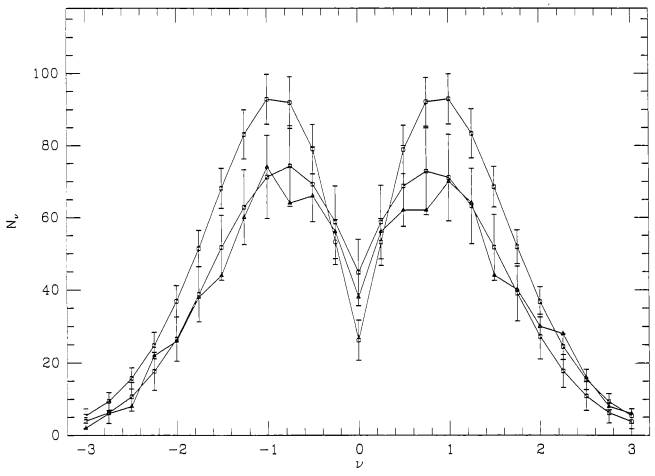

FIG. 3.—Number of spots normalized to the area of the sphere including cold and hot spots. Upper curve is for noise maps alone (*open squares*). The other curve (*open squares*) is for maps generated with noise and cosmological fluctuations with a Harrison-Zeldovich spectrum (16 μK normalization). Superposed is the data obtained from the 53(A + B) DMR maps (*filled triangles*).

TABLE 1

χ^2 AND ITS PROBABILITY FOR NUMBER OF SPOTS AND GENUS OF *COBE*-DMR MAPS

Map	χ^2_N	$P(\chi^2 \geq \chi^2_N)$	χ^2_G	$P(\chi^2 \geq \chi^2_G)$
53	0.62	95.4	0.72	83.3
90	1.48	13.9	1.73	8.4
5390	1.03	47.1	1.03	47.1
53	6.75	<1/400	7.51	<1/400
90	3.59	<1/400	4.38	<1/400

NOTE.—The first three rows are the χ^2 statistic (5) for the number of spots χ^2_N and genus χ^2_G and their probabilities (%) when the Harrison-Zeldovich hypothesis is assumed. The 5390 entry refers to the statistics of the weighted averaged map of DMR 53 and 90 sum maps. Last two rows give the same statistics when the null hypothesis is assumed in the Monte Carlo procedure.

tistical test and the discrimination efficiency of a topological descriptor. Noisy maps have noise and signal curves in close proximity. L_ν and A_ν have such close noise and signal curves and so cannot discriminate between power spectra with indices near one. Genus and hot spot number are the only descriptors used to test hypothesis.

To compare *COBE*-DMR data with cosmological models χ^2 and the cumulative probability distribution of χ^2 are constructed from Monte Carlo data (Gott et al. 1992). For each Monte Carlo map the topological descriptor values U_ν evaluated at 25 thresholds ν: $-30 \ldots 3.0$ are used to compute

$$\chi^2 = \frac{1}{24} \sum_{j=1}^{25} \frac{(U_j - \langle U_j \rangle)^2}{\sigma_j^2}, \qquad (5)$$

where $\langle U_j \rangle$ and σ_j are calculated from the Monte Carlo simulations for that cosmological model. Table 1 shows the χ^2 and probabilities for the 53 and 90 sum maps and the weighted average.

5. PREPARATION OF DATA

In this analysis four of the six DMR sky maps—53-A, -B, 90-A, and -B—are used. The data is in the sky cube format using Geocentric Ecliptic coordinates. Before the topological analysis the dipole and 2 μK kinematic quadrupole components are removed, the maps are rotated to galactic equatorial coordinates, and to reduce noise the maps have an additional Gaussian smoothing of 2°.9. An equatorial band of $|b| < 30°$ is excluded from the analysis. Cosmological hot and cold spots will exist in all four maps as unresolved sources, so a weighted average of the four maps is made to reduce the noise.

As a data integrity and analysis software check the dipole, rms 10° sky variation, and quadrupole are computed and compared with *COBE* results. The dipole and quadrupole are obtained by a least-squares fit of the harmonic expansion to the map and are in agreement with Smooth et al. (1992).

6. ANALYSIS AND CONCLUSIONS

Figure 1, a plot of a_ν versus ν, illustrates what would be obtained for a pure random field independent of its coherence angle. In the same figure, a versus threshold for the 31 GHz DMR sum map, shows large deviations which increase with decreasing galactic cut indicating galactic contamination at high latitudes. For the 53 and 90 sum maps, no deviations beyond 1 σ of Figure 1 are seen above 25°.

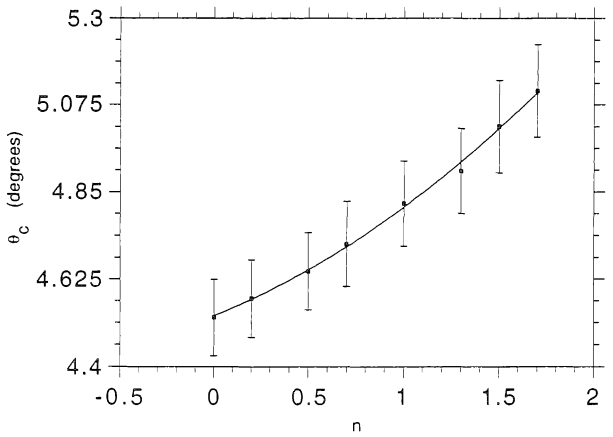

FIG. 4.—Coherence angle versus spectral index as obtained from the Monte Carlo runs. Solid curve is a fit to a parabola.

Genus and number of spots were used to test for the consistency of a primordial Harrison-Zeldovich perturbation spectrum. The null hypothesis that the structure in *COBE* maps is due solely to instrumental noise is rejected with high confidence, as seen in Table 1 and Figure 3. The contribution from known infrared, radio, and X-ray point sources is negligible (Bennett et al. 1993), so the observed structure must be of cosmological origin.

Genus and number of spots computed on Monte Carlo realizations of CMB maps with a Harrison-Zeldovich power spectrum normalized to 16 μK $Q_{\rm rms}$ are found to be consistent with DMR data to a high confidence, as seen in Table 1, as are other spectral indices. To see the genus dependence on the spectral index, several sets of Monte Carlo realizations are generated with fixed $Q_{\rm rms}$ normalization and variable n. For each index the genus curve as a function of threshold ν is fitted using equation (2) to obtain the best θ_c. The coherence angle dependence on spectral index is almost linear, as seen in Figure 4. With θ_c errors obtained from Monte Carlo simulations the best value of n is found by fitting the *COBE* genus curves to determine their coherence angle which for the 53 GHz sum DMR map is 4.9 ± 0.1 which implies a 1.2 ± 0.3 spectral index in agreement with Smoot et al. (1992) using a ACF fit.

I thank W. P. Trower for his suggestions and help in editing the manuscript, R. Ruffini, L. Cayón, R. Fabbri, A. Kogut, E. Martínez-González, and G. Smoot for many useful comments and conversations. This work has been supported by Colciencias of Colombia project No. 1204-05-012-91, and the European Community under contract No. CI1-CT92-0013. The support of the SuperComputer Computations Research Institute of Florida State University, where some of the Monte Carlo runs were done, is greatly appreciated. The *COBE* datasets were provided by the NSSDC.

REFERENCES

Adler, R. J. 1981, The Geometry of Random Fields (New York: Wiley)
Bennett, C., et al. 1993, ApJ, 414, L77
Bennett, D. P., Stebbins, A., & Bouchet, F. R. 1992, ApJ, 399, L5
Bond, J. R., & Efstathiou, G. 1987, MNRAS, 226, 655
Cayón, L., Martínez-González, E., & Sanz, J. L. 1991, MNRAS, 253, 599
Coles, P. 1988a, MNRAS, 231, 125
———. 1988b, MNRAS, 234, 509
Coles, P., & Barrow, D. 1997, MNRAS, 228, 407

Gott, J. R., et al. 1990, ApJ, 352, 1
Gurzadyan, V., & Torres, S. 1993, in The Present and Future of the Cosmic Microwave Background, ed. E. Martínez-González, L. Cayón, & J. L. Saez, in press
Harrison, E. R. 1970, Phys. Rev. D, 1, 2726
Martínez-González, E., & Sanz, J. L. 1989, MNRAS, 237, 939
Park, C., Spergel, D. N., & Turok, N. 1991, ApJ, 372, L53
Sachs, K., & Wolfe, A. M. 1967, ApJ, 147, 73
Sazhin, M. V. 1985, MNRAS, 216, 25p
Scaramella, R., & Vittorio, N. 1988, ApJ, 331, L53
———. 1990, ApJ, 353, 372
Smoot, G. F., et al. 1991, ApJ, 371, L1
———. 1992, ApJ, 396, L1
Torres, S., et al. 1989, in Data Analysis in Astronomy 1988, ed. V. di Gesu, L. Scarsi, & M. C. Maccarone (New York: Plenum), 319
Vittorio, N., & Juszkiewicz, R. 1987, ApJ, 314, L29
Zeldovich, Ya. B. 1972, MNRAS, 160, 1P